Inhomogeneous free layer in perpendicular magnetic tunnel junctions and its impact on the effective anisotropies and spin transfer torque switching efficiency

A. A. Timopheev,[1,*] B. M. S. Teixeira,[2] R. C. Sousa,[1] S. Aufret,[1] T. N. Nguyen,[1] L. D. Buda-Prejbeanu,[1] M. Chshiev,[1] N. A. Sobolev,[2,3] and B. Dieny[1]

[1]*Université Grenoble Alpes, CEA, CNRS, Grenoble INP, INAC, SPINTEC, F-38000 Grenoble, France*

[2]*Physics Department & i3N, University of Aveiro, 3810-193 Aveiro, Portugal*

[3]*National University of Science and Technology "MISiS", 119049 Moscow, Russia*

(Received 26 January 2017; revised manuscript received 8 May 2017; published 10 July 2017)

Magnetoresistive and magnetoresonance measurements carried out on patterned perpendicular magnetic tunnel junction pillars and full-sheet films reveal magnetic inhomogeneities of FeCoB free layer grown on MgO and coated with Ta. At low FeCoB thicknesses, the layer behaves as an ensemble of weakly coupled grains resulting in a decrease of the free-layer thermal stability. In contrast, for thicker layers, the grains become more strongly coupled but strong magnetic inhomogeneities remain, yielding the emergence and further increase of a second-order magnetic anisotropy term ($\sim K_{2\text{eff}}\cos^4\theta$), eventually resulting in an easy-cone anisotropy. We show that the static and dynamic magnetic properties of such a free layer can be successfully described by a granular model with three thickness-dependent parameters: mean perpendicular anisotropy of the grains, grain-to-grain anisotropy distribution, and intergrain exchangelike coupling strength. Easy-cone anisotropy may help reduce the stochasticity of the spin transfer torque switching. However, it arises at intermediate values of the intergrain exchange coupling where the spin transfer torque (STT) switching efficiency is degraded, as shown by multimacrospin modeling. This is due to the excitation of exchange modes contributing weakly to the STT switching process while dissipating part of the STT energy.

DOI: 10.1103/PhysRevB.96.014412

I. INTRODUCTION

An important issue in conventional spin transfer torque magnetic random access memory (STT-MRAM) is associated with the stochasticity of the switching. Indeed, a misalignment between the storage layer magnetization and reference layer magnetization is required to trigger the switching induced by spin transfer torque. In real perpendicular magnetic tunnel junction (pMTJ) devices, a finite thermal stability of the free layer provides this necessary initial misalignment. Thermal fluctuations, being random by nature, cause a broad distribution of switching times which is detrimental for the device performance. Micromagnetic distortions of the free layer at the pillar edges can also provide the required noncollinearity, but these are technologically challenging to control, since the pillar edges contain significant structural and magnetic defects introduced by the nanofabrication process. It is therefore highly desirable to have a well-controlled source of misalignment inside the free layer itself.

A magnetic "easy-cone" state would be a solution to the problem described above: the initial misalignment is set by the cone angle, while the precession orbit plane during the STT switching would be always perpendicular to the polarizer, thus representing a very efficient configuration for the absorption of the STT energy. Such easy-cone anisotropy is observed, for instance, in bulk $NdCo_5$ [1,2] compounds. Phenomenologically, the magnetic easy-cone state implies the presence of a higher-order anisotropy term with a negative constant. Thus, if in zero magnetic field the magnetic free energy of a thin-film ferromagnet has the form $E = -K_{1\text{eff}}\cos^2\theta - K_{2\text{eff}}\cos^4\theta$, θ being the angle between the magnetization and the normal to the plane of the layers, an easy-cone anisotropy arises when the following conditions are fulfilled: $K_{1\text{eff}} > 0, K_{2\text{eff}} < 0$, and $-K_{2\text{eff}}/K_{1\text{eff}} > 0.5$. The cone angle θ_C is then given by $\cos^2\theta_C = -K_{1\text{eff}}/(2K_{2\text{eff}})$. An analytical study [3] and macrospin simulations [4] have shown a noticeable improvement in the switching characteristics of the free layer in the easy-cone state, especially in terms of reduction of the stochasticity of the reversal. One should notice that the second-order anisotropy is important not only in the easy-cone state but also in the regime where the second order anisotropy is weak so that the system is still in the perpendicularly magnetized state [5]. Moreover, the second-order anisotropy is useful not only for STT-MRAM but also for spin torque oscillator [6]. Recently, a second-order magnetic anisotropy with negative constant has been observed in FeCoB/MgO systems [7–9]. The easy-cone magnetic state has also been found at room temperature in Ta/FeCoB/MgO films [7,8] with FeCoB thickness close to the anisotropy reorientation transition between in-plane and out-of-plane.

It was proposed that a possible origin of the second-order anisotropy in FeCoB/MgO lies in the spatial inhomogeneity of the first-order anisotropy [10]. However, various magnetic parameters (anisotropy, exchange, and/or magnetic moment) can in principle influence the second-order anisotropy constant and their relative importance is not yet clear. In FeCoB/MgO systems, a local reduction of the interfacial anisotropy may naturally appear at grain boundaries due to local segregation during the crystallization process of all the chemical elements thermodynamically insoluble in the crystalline FeCo host. This is true not only for FeCo but also for the MgO crystallization process that can alter the electrical properties of the tunneling barrier. Also, enhanced diffusion of atoms from the neighboring nonmagnetic metallic layers, such as Ta or other capping materials, may preferentially occur along the

*andrey.timopheev@gmail.com

grain boundaries during the annealing process. This will affect both the magnetic anisotropy and strength of intergranular coupling. The exchange stiffness at grain boundaries will be reduced as compared to the intragrain exchange. Even an ideally clean MgO/FeCo interface may exhibit a periodic array of dislocations releasing the elastic stress accumulated due to the misfit between the FeCo and MgO lattices. Regardless of the source of spatial fluctuations in interfacial anisotropy, the same phenomenological model can be used to investigate the macroscopic magnetic properties of the storage layer. This model consists in describing the system as an ensemble of exchange-coupled grains having different effective perpendicular anisotropy fields.

In this paper, we investigate experimentally, by magnetotransport and ferromagnetic resonance (FMR) measurements, the magnetic properties of FeCoB storage layer grown on MgO and coated by Ta, widely used in pMTJ stacks. We have found that the storage layer is magnetically inhomogeneous and exhibits a granular behavior for thickness below ∼1.3 nm. Based on the granular model mentioned above, we analyze the thickness-dependent evolution of the magnetoresistive and magnetoresonance properties of full-sheet MgO/FeCoB/Ta films and pMTJ pillars having the identical MgO/FeCoB/Ta storage layer. We show how the higher-order anisotropy term, $K_{2\mathrm{eff}}\cos^4\theta$, in FeCoB layer can be correlated with the structural parameters characterizing the inhomogeneity of this layer. Furthermore, we study the impact of the granular nature of the storage layer on its switching characteristics as a function of the intergrain exchange coupling using a multimacrospin simulation approach. In the context of STT-MRAM, it was previously shown [4] that the higher-order anisotropy term in the storage layer can help reduce the stochasticity of the switching thanks to the onset of an easy-cone anisotropy. This paper shows that the micromagnetic nature of this second-order anisotropy term provokes degradation of the spin transfer torque efficiency due to additional energy dissipation associated with the excitation of exchange modes in the storage layer.

II. SAMPLES DESCRIPTION AND EXPERIMENTAL TECHNIQUES

Full pMTJ stacks of composition Ta(1)/Pt(5)/[Co(0.5)/Pt(0.25)]$_6$/Co(0.5)/Ru(0.9)/[Co(0.5)/Pt(0.25)]$_3$/Co(0.5)/Ta(0.3)/$Fe_{72}Co_8B_{20}$(1.2)/MgO/($Fe_{72}Co_8B_{20}$)(t_{FeCoB})/Ta(1)/Pt(2)/Ru(2) and half pMTJ of composition Ta(3)/$Fe_{72}Co_8B_{20}$(0.4)/MgO/($Fe_{72}Co_8B_{20}$)(t_{FeCoB})/Ta(1)/Pt(3), allowing investigation of the properties of the storage layer only, were deposited by magnetron sputtering. The numbers in parentheses are nominal thicknesses of the deposited material in nanometers. The free (storage)-layer thickness, t_{FCB}, was varied between 1.0 and 1.8 nm. We do not make any assumptions about the magnetic dead-layer thickness and its variation with the total film thickness. The tunneling barrier was formed by natural oxidation, i.e., exposing the deposited magnesium layer to an oxygen atmosphere. For the samples used in this study, the deposited magnesium thickness was 1.3 nm. The multilayers were annealed at $T = 300\,^{\circ}\mathrm{C}$. The full pMTJ stacks were then patterned in the form of pMTJ pillars of various diameters ranging between 150 and 30 nm. Other details can be found in Ref. [11]. Tunnel magnetoresistance (TMR) measurements at room temperature were performed afterward using an automated wafer prober. In addition, individual pMTJ pillars were measured using a physical property measurement system (PPMS, Quantum Design) at temperatures from 4 to 400 K and with the magnetic field applied perpendicular to the sample plane. Finally, *X*-band FMR spectrometry was performed to study magnetic properties of the free-layer films. A macrospin model was used to fit the angular dependence of the FMR field in order to extract the magnetic anisotropy effective fields. A more detailed description of the FMR experimental technique and the fitting procedure can be found in Ref. [2].

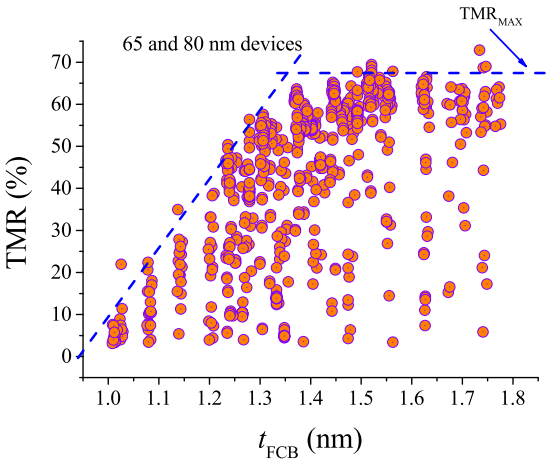

FIG. 1. Room-temperature TMR as a function of the free-layer thickness (t_{FCB}). Measurements were performed on 825 patterned devices for which the nominal thickness of MgO was 1.3 nm.

III. MAGNETORESISTIVE PROPERTIES

Figure 1 shows the measured TMR values of more than 800 pMTJ pillars having different free-layer thicknesses between 1.0 and 1.8 nm. The nanofabrication process results in electrical shunts across the MgO barrier reducing the measured TMR magnitude in some of the patterned devices. As a consequence, for a given free-layer thickness, one can observe a distribution of device-to-device TMR values within the range (0, TMR$_{\mathrm{max}}$), where TMR$_{\mathrm{max}}$ would ideally correspond to the case of an "undamaged pillar". Indeed, TMR$_{\mathrm{max}}$ will be limited by the effective spin polarization in the pMTJ system. Thanks to the large number of measured pMTJ elements we can easily draw an envelope of the TMR distribution, representing the highest observed TMR at each FeCoB thickness. By following this high-TMR edge as a function of the free-layer thickness, one can observe two regions separated by a characteristic thickness $t_{\mathrm{FCB}} \sim 1.3$ nm. Below this value, the TMR$_{\mathrm{max}}$ value increases with the free-layer thickness, while above it the TMR amplitude remains constant. This dependence can be attributed to the thickness dependence of the effective spin polarization of the whole pMTJ system at room temperature. Considering that the tunneling barrier and the polarizer layer underneath are not affected by the free-layer thickness, which is a reasonable assumption for bottom-pinned pMTJ structures, the variation of the effective spin polarization in the pMTJ system can be

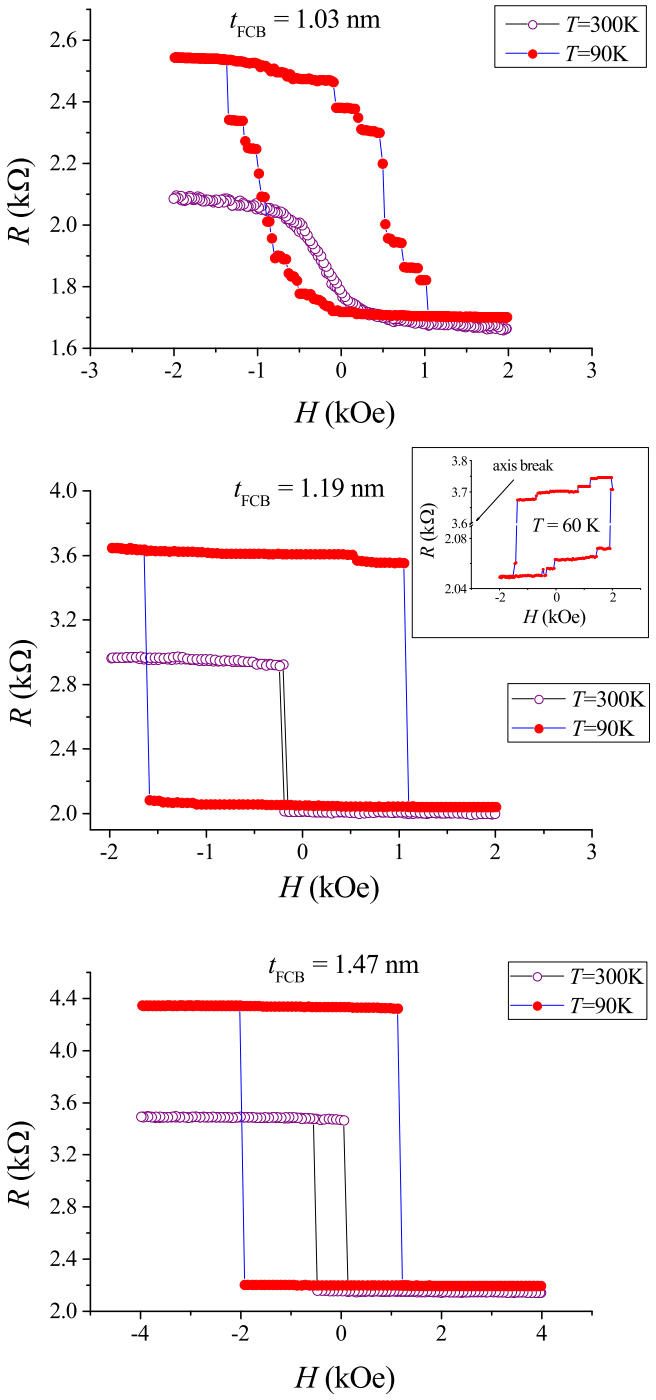

FIG. 2. Out-of-plane magnetoresistance loops measured on pMTJ pillars with a nominal diameter of 80 nm and three different free-layer thicknesses (t_{FCB}). The selected devices were cut out from the wafer, wire bonded to the measurement chip, and placed into the PPMS chamber.

entirely ascribed to the magnetic and structural properties of the free layer.

We have chosen several pMTJ devices with different free-layer thicknesses and almost identical nominal thickness of MgO for a temperature-dependent study. Figure 2 shows magnetoresistance loops at $T = 300$ and 90 K for three samples with thicknesses of 1.03, 1.19, and 1.47 nm, respectively. A clear influence of the free-layer thickness on the evolution of the shape of these MR loops with temperature is observed. For the pMTJ having the thickest free layer (1.47 nm), the loops are square-shaped at all temperatures, indicating that the whole free layer switches in one step. In contrast, for the pMTJs with thinner free layers, a different behavior is observed involving successive jumps at low temperatures. This reveals a granular nature of these thin free layers. This granularity can be associated with a tendency toward island growth during the deposition of the FeCoB layer on MgO and/or to a strongly reduced exchange stiffness across the grain boundaries due to local segregation of nonmagnetic elements at these boundaries, as previously mentioned. Due to this granular structure, the thermal stability of the free layer is strongly reduced. As a matter of fact, if the thin film were continuous, a higher effective anisotropy would be expected since $K_{\text{eff}} = K_s/t - 2\pi M_s^2$, resulting in a higher thermal stability factor Δ, K_s (surface perpendicular anisotropy constant). However, if the free layer breaks into an ensemble of weakly exchange-coupled grains, the effective nucleation volume entering the thermal stability factor is significantly smaller than for continuous film. In our case a clear signature of granularity of the free layer appears below a nominal thickness of 1.3 nm through the multistep behavior of the hysteresis loops.

Figure 3 shows the temperature dependence of the TMR and resistance in the parallel state (*Rp*) for these devices. The temperature dependence of *Rp* is weak (2.5% over the 200 K range) and has the same slope for all three devices. This allows us to conclude that the tunneling barrier is not much affected by the granularity of the free layer. It also supports the interpretation of the experiments shown in Fig. 2, i.e. only the free-layer properties change with the free-layer thickness. The weak negative temperature coefficient (approximately -1.2×10^{-4} K^{-1}) indicates no pinholes in the barrier [12] and can be ascribed to the thermal smearing of the tunneling electron Fermi-Dirac energy profile [13]. At the same time, the TMR amplitude of the pillar with $t_{FCB} = 1.03$ nm does not reach the same magnitude as that of the pMTJs with the thicker free layer even at low temperatures, indicating that the effective polarization is still much lower for the thinner free layer. This effect can be attributed to residual thermal fluctuations, but also to the fact that only a part of the FeCoB/MgO interface is covered by the ferromagnetic material with a strong spin polarization (FM grains). The weakly magnetic material accumulated at the grain boundaries emits a current with lower spin polarization than the magnetic material in the inner part of the grains, yielding on average a reduced TMR amplitude. The temperature dependences of TMR in these devices are quite linear in the 90–300 K temperature range. Their extrapolation to the "zero-TMR" temperature indicates the temperature at which the spin polarization vanishes due to excessive thermal fluctuations in the free layer. As expected, it occurs at lower temperatures for thinner free layers.

IV. FERROMAGNETIC RESONANCE ON FULL-SHEET FREE LAYER

Ferromagnetic resonance was employed to further understand the phenomenon of free-layer granularization.

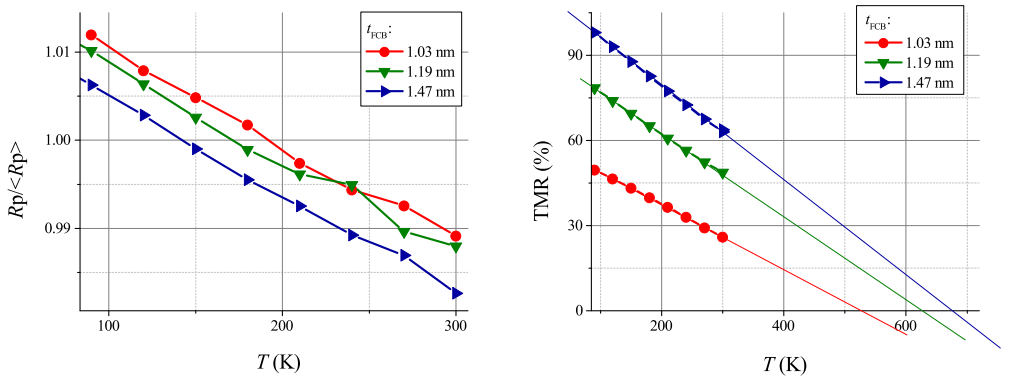

FIG. 3. Left panel: Temperature dependences of the resistance of pMTJ pillars with various free-layer thicknesses in the parallel state, *Rp*. Right panel: TMR for the selected devices. Since the absolute *Rp* value is fluctuating from device to device due to deviations of the actual device diameter from its nominal value, here we show the resistance of the device normalized to the mean value $\langle Rp \rangle$ of all the *Rp* points measured for a given device.

A MgO/FeCoB/Ta sandwich film comprising an FeCoB wedge was cut into small pieces, small enough so that the thickness gradient can be considered as negligible (±0.18 A) in each of them. Field-swept FMR spectra were measured as a function of the magnetic field angle (θ_H) counted from the sample normal. The linewidth (ΔH) and resonance field value (H_{res}) of the FMR lines were extracted. A macrospin model was fitted to $H_{res}(\theta_H)$ in order to extract the effective magnetic anisotropy fields of the films.

Figure 4 shows the FMR spectra at various magnetic field angles (10° angular step) for a film with $t_{FCB} = 0.94$ nm. Even for this very thin film, the FMR angular variation at $T = 300$ K clearly reveals a quite large effective perpendicular anisotropy field $2K_{eff}/M_s \sim 3$ kOe. This means that despite the fact that the free layer is formed of weakly coupled grains and is thermally unstable (which is suggested by Fig. 2), the ferromagnetic grains themselves still preserve a strong perpendicular anisotropy.

With increasing FeCoB film thickness, the amplitude of the $H_{res}(\theta_H)$ variation decreases, as expected due to the increasing role of the demagnetizing energy counterbalancing the perpendicular anisotropy from the MgO/FeCoB interface. The film thickness range used in Fig. 5 covers the whole transition of the magnetic anisotropy from "perpendicular easy axis" to "easy plane". Near the anisotropy reorientation transition, a second-order anisotropy term is recognized directly from the $H_{res}(\theta_H)$ dependences. In our previous work [7], as well as in several others [8,9], such a higher-order contribution, $K_{2eff}\cos^4\theta$, was observed in full-sheet MgO/FeCoB/Ta films, as well as in patterned pMTJ pillars. The K_{2eff} constant has a negative sign, while the first term, $K_{1eff}\cos^2\theta$, is positive. This can lead to the formation of an easy-cone magnetic ground state, in which the magnetization is tilted away from the film normal by a certain angle. The anisotropy energy is then invariant by rotation around the cone axis. In this particular film, at $T = 300$ K the easy-cone state is observed for the film with $t_{FCB} = 1.63$ nm.

The extracted effective fields corresponding to the first- and second-order anisotropy constants, K_{1eff} and K_{2eff}, are reported in Fig. 6. Here $K_{1eff} = K_{1s}/t_{FeCoB} - 2\pi M_s^2$ with the surface anisotropy constant K_{1s}. One can observe quite different thickness behavior for K_{1eff} and K_{2eff}. As the FeCoB

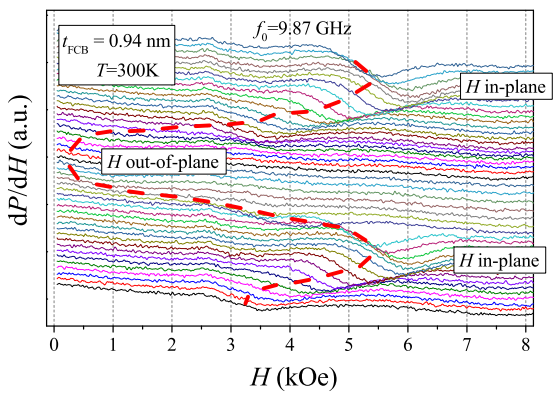

FIG. 4. FMR spectra collected as a function of the angle between the external magnetic field and film normal (i.e., out-of-plane angular dependences). The angular step is 10°. The dashed red line is a guide for the eye showing an approximate angular variation of the FMR field.

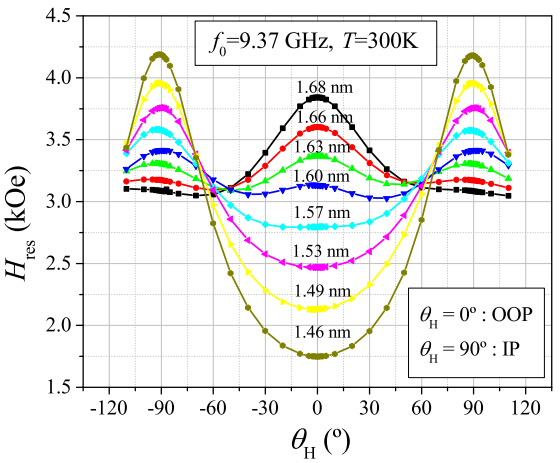

FIG. 5. Room-temperature angular dependences of the FMR resonance field extracted from the measured spectra. The free-layer thickness is shown atop each dependence.

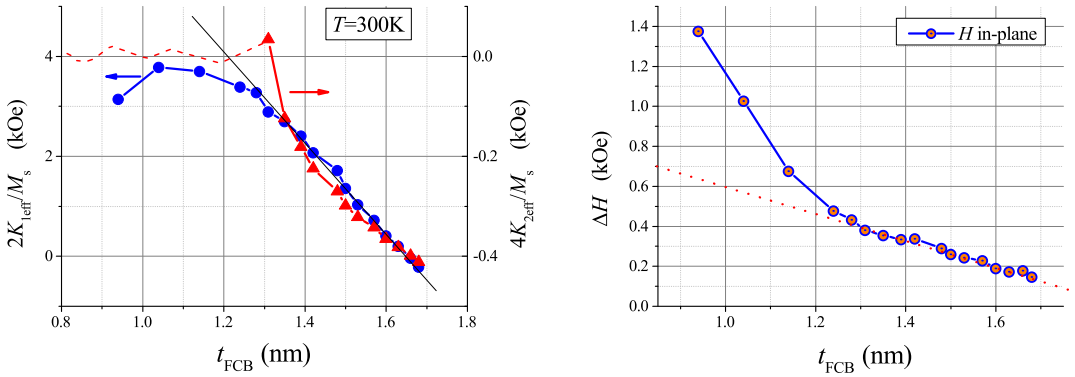

FIG. 6. Left panel: Thickness dependence of the $K_{1\text{eff}}$, $K_{2\text{eff}}$ constants extracted from the angular dependences of FMR resonance field (example shown in Fig. 5). Right panel: FMR linewidth (full width at half maximum, FWHM) versus free-layer thickness. A significant increase is observed below 1.3 nm.

thickness is reduced, $K_{1\text{eff}}$ increases almost linearly (actually, it should increase as $1/t_{\text{FCB}}$, but due to the narrow thickness range, it looks like linear versus t_{FCB}), then starts deviating from this trend below $t_{\text{FCB}} = 1.3$ nm. At lower thicknesses, $K_{1\text{eff}}$ levels off and then starts decreasing again. In this range of thicknesses, the tendency toward island formation can lead to an effective thickness of the grains larger than the nominal thickness by conservation of the amount of deposited material. In addition, due to the weak intergrain coupling already discussed for these thin free layers, the role of thermal fluctuations at room temperature may be enhanced compared to thicker free layers, yielding also a lower effective anisotropy for a given nominal thickness. In particular, for the films with $t_{\text{FCB}} < 1$ nm the decrease in $K_{1\text{eff}}/M_s$ can be readily ascribed to thermal fluctuations inside each grain—-a superparamagnetic regime of FMR is observed [14]. The significant increase in the linewidth observed for $t_{\text{FCB}} <$ 1.3 nm (Fig. 6) further supports the idea of a granular-type behavior of the thin free layers. The grain-volume distribution and the associated grain-to-grain distribution of effective perpendicular anisotropy fields are expected to be broader than for continuous films of the same nominal thickness. Weak intergrain exchange also causes each grain to resonate independently of each other; dynamic dipole-dipole coupling can be non-negligible in this case, further increasing the FMR line broadening.

At the same time, $K_{2\text{eff}}$ amplitude decreases in absolute value with decreasing film thickness. We cannot estimate its magnitude below $t_{\text{FCB}} = 1.3$ nm because it becomes too small compared to $K_{1\text{eff}}$ and because of the strong broadening of the FMR signal at these very small thicknesses. It is assumed therefore that $K_{2\text{eff}} \approx 0$ for $t_{\text{FeCoB}} < 1.3$ nm.

Referring to the micromagnetic nature of this higher-order term (spatial fluctuations of the uniaxial anisotropy), its thickness dependence can be explained as follows. Dieny and Vedyayev [10], and recently Sun [15], have shown that two exchange-coupled magnetic systems having different uniaxial anisotropies can exhibit a higher-order anisotropy term, $K_{2\text{eff}}\cos^4\theta$, with a negative $K_{2\text{eff}}$ constant. Similarly, our magnetic storage layer can be approximated by an ensemble of macrospins (individual FM grains) having grain-to-grain distribution of the $K_{1\text{eff}}$ parameter. The grains are coupled by intergrain exchange, whose strength depends on the nominal film thickness. The first extreme case corresponds to the situation of zero intergrain coupling. Here, the FMR technique will see only the first-order anisotropy and inhomogeneous FMR line broadening. The second limiting case corresponds to a strongly coupled ensemble of grains. Correspondingly, the FMR will excite only a uniform precession mode in an effective field which corresponds to an average of the anisotropy fields over the whole ensemble of grains. All the spins behave as a single macrospin, and the exchange energy, as in the case of a traditional ferromagnet, does not appear in the effective field functional defining the resonance frequency. In between these two regimes lies the region of interest, where the intergrain coupling influences the grain dynamics, thus yielding higher-order precession modes. The relative weight of the intergrain exchange energy in the total magnetic free energy of the system actually determines the magnitude of this second-order anisotropy contribution.

Varying the nominal film thickness allows tuning the intergrain coupling strength in our samples. The increase of the nominal FeCoB thickness reduces the amplitude $\Delta K_{1\text{eff}}$ of the spatial fluctuations of $K_{1\text{eff}}$. At the same time, it strongly increases the intergrain coupling strength. The imbalance between these two opposing effects actually yields a negative increase of $K_{2\text{eff}}$ with increasing FeCoB thickness. A leveling off and even a decrease of $K_{2\text{eff}}$ is expected at even larger thicknesses, but this is outside the thickness range considered for magnetic memory applications.

The temperature dependences of the extracted effective anisotropy fields for several free-layer thicknesses are shown in Fig. 7. $K_{1\text{eff}}$ increases at low temperature as expected in the case of a pure single-ion magnetocrystalline anisotropy, whose temperature dependence, according to the Callen and Callen theory [16,17], can be described as a power law of the saturation magnetization, $M_s(T)$. Because FMR experiments give the effective anisotropy fields rather than the anisotropy constants, it is hard to separate the temperature dependence of the true surface anisotropy $K_s(T)$ contribution from the magnetostatic part $2\pi M_s^2(T)$ without additional magnetostatic measurements. Nevertheless, the increase of M_s with decreasing T is confirmed by many experiments performed on nanometer-thick FeCo films (see, for example, Refs. [18,19]). Assuming the same behavior in our samples, we can conclude that K_s also increases with decreasing T according to a power

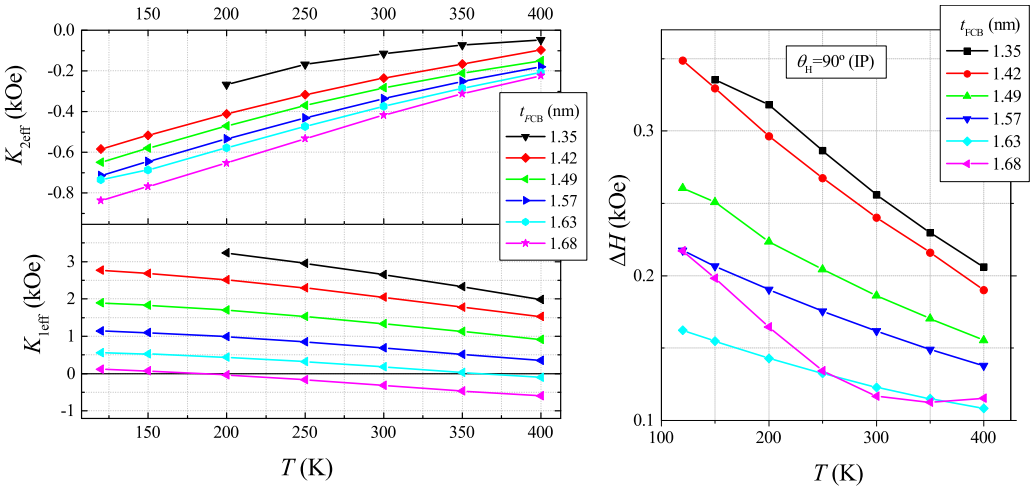

FIG. 7. Left panel: Temperature dependence of the $K_{1\text{eff}}$, $K_{2\text{eff}}$ constants for the sample with different thicknesses of the free layer. Right panel: FMR linewidth (FWHM) versus temperature measured with the in-plane magnetic field.

law, $K_s \sim M_s^n(T)$, with $n \geqslant 2$. Therefore, the experimentally observed increase of $K_{2\text{eff}}$ is in line with the Dieny-Vedyayev model [10] predicting an increase of $K_{2\text{eff}}$ with increasing amplitude of spatial fluctuations $\Delta K_{1\text{eff}}$. The $K_{1\text{eff}}$ increase not only raises the $K_{2\text{eff}}$ amplitude, but also contributes to the FMR broadening (Fig. 7) observed at low temperatures. This is again an expected behavior associated with the micromagnetic origin of the higher-order anisotropy term: $K_{2\text{eff}}$ and FMR linewidth are expected to vary similarly as a function of the spatial fluctuations of $K_{1\text{eff}}$.

Let us summarize our experimental findings. By analyzing the thickness dependence of the magnetoresistive and magnetoresonance properties of the free layer, we have observed a gradual evolution of the free-layer behavior from continuous-film behavior at large FeCoB thicknesses (>1.3 nm) toward an ensemble of weakly coupled grains (<1.3 nm) for thin FeCoB layers. Reducing the thickness of the latter yields a strong decrease of the intergrain exchange coupling and an increase in the grain-to-grain $K_{1\text{eff}}$ distribution, $\Delta K_{1\text{eff}}$. For $t_{\text{FCB}} <$ 1.3 nm, the free layer can be viewed as an ensemble of weakly coupled grains with an effective perpendicular anisotropy field exceeding 3 kOe. The grains are still strongly ferromagnetic but quite small in volume and therefore thermally unstable, resulting in nonhysteretic magnetoresistance loops at $T =$ 300 K and multistep reversal hysteresis loops at $T <$ 100 K. Fluctuations of the grain thickness (within one monolayer) result in a noticeable distribution of the effective perpendicular anisotropy fields from grain to grain.

The tunneling barrier below the free layer is not noticeably affected by the granular nature of the free layer. Similar temperature dependence and resistance values in the parallel state are observed for the magnetic layers having a granular structure as compared to those forming a continuous film. Degradation of the maximum TMR value in thinner films is therefore linked with thermal fluctuations in the grains and to the partial coverage of the tunneling barrier by the materials with a high spin polarization (the inner part of the grains). Due to local accumulation of nonmagnetic species in the grain boundaries, particularly Ta, its corresponding area emits tunnel electrons which are less spin-polarized, resulting in a reduced TMR amplitude. These areas also locally yield a reduced interfacial anisotropy and a reduced exchange stiffness constant.

Increasing the nominal thickness produces two effects: an increase of the intergrain exchange and a decrease of the amplitude $\Delta K_{1\text{eff}}$ of the spatial fluctuations of $K_{1\text{eff}}$. Both effects result in a gradual decrease of the inhomogeneous FMR line broadening. With increasing FeCoB thickness, because the intergrain coupling field H_{IC} increases faster than the fluctuations amplitude $\Delta K_{1\text{eff}}$ decreases ($1/t$ dependence), $K_{2\text{eff}}$ constant increases in negative values. The micromagnetic nature of this higher-order contribution makes the $K_{2\text{eff}}$ parameter depend on the $\Delta K_{1\text{eff}}$ to H_{IC} ratio as expected from the Dieny-Vedyayev model [10]. As evidenced by temperature-dependent FMR experiments, the inhomogeneous broadening is the main mechanism defining the FMR linewidth for all the free-layer thicknesses studied here.

An important question which naturally follows from this experimental study is how the granular nature of the free layer influences its STT switching characteristics. In case of a pure macrospin switching, three main parameters influence the switching properties: magnetic anisotropy, spin torque efficiency, and damping. It was shown theoretically and by modeling [4] that the presence of a negative second-order anisotropy term ($K_{2\text{eff}}$) in the free layer improves the switching characteristics by reducing the stochasticity of the switching process [3,20]. Similarly, it might be possible to benefit from the granular nature of the free layer in terms of STT switching characteristics. This assumption was investigated by multimacrospin simulations and reported in the next section.

V. MODELING: MULTIMACROSPIN APPROACH

As a toy model, we described the storage layer as a system of four exchange-coupled macrospins. The four grains are assumed to have identical volume (400π nm^3), Gilbert damping ($\alpha = 0.012$), and saturation magnetization ($M_s = 1000$ emu/cm^3), but different $K_{1\text{eff}}$, which is reflected in the different effective perpendicular anisotropy fields ($2K_{1\text{eff}}/M_s = 3.0, 3.3, 2.5, 2.0$ kOe). The ensemble is subjected to random thermal fluctuations, in line with Brown's

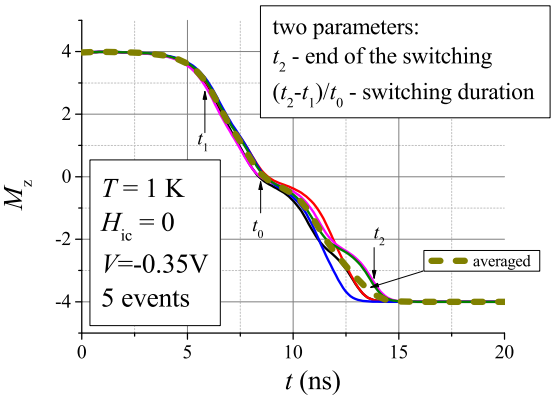

FIG. 8. Simulation of five STT switching events of the ensemble, their average (dotted thick line), and characteristic points on the averaged dependence which are used to extract timing parameters of the switching process.

theory [21] by introducing a temperature stochastic term in the Landau-Lifshitz-Gilbert (LLG) equation. Finally, each macrospin is subjected to the dampinglike STT with a linear prefactor of 150 Oe/V. In these simulations, only two parameters are varied: the effective exchange field, H_{IC}, acting on each grain and resulting from the intergrain coupling with the three other grains, and the amplitude of the thermal fluctuations. For each set of parameters, a full switching event, i.e., all four grains in the ensemble being reversed, is repeated 100 times, and the averaged curve is analyzed in terms of two output parameters (see Fig. 8): (i) the relative switching duration, which is just a switching time distribution width $(t_2 - t_1)$ of the averaged curve normalized by the mean switching time (t_0); (ii) time necessary to switch the whole ensemble, t_2. Both characteristics are essential for the characterization of the writing performance of real pMTJ memory elements.

Figure 9 shows how these two timing parameters evolve versus writing voltage at $T = 300$ K. Whatever the intergrain coupling strength, the switching dynamics gets faster with increasing writing voltages as commonly observed in the STT switching dynamics. This is true for the distribution of switching times $(t_2 - t_1)$ of the individual grains, for their mean value $(\sim t_0)$, as well as for their ratio. It was found empirically that the relative switching duration follows a $1/V$ law, where V is the writing voltage. The deviation at $V < -0.35$ V for $H_{IC} = 0$ is linked with the fact that the most stable grain with $2K_{1eff}/M_s = 3.3$ kOe is not fully statistically switched anymore (switching probability $< 100\%$) within the given writing pulse width of 250 ns. Once the grains are exchange-coupled, the three less-stable grains, having been switched by STT, decrease the switching threshold voltage for the most stable grain, thus the dependence continues following the $1/V$ law. Interestingly, for the higher writing pulse voltages ($V \geqslant 0.35$ V), where all the grains in the ensemble are being switched regardless of the coupling strength, moderate coupling results in the longer switching duration than in the uncoupled and/or strongly coupled case. The full switching time (right panel in Fig. 9) is also observed to be the longest for moderate intergrain coupling. Following an almost perfect $\ln(t_2) \sim 1/V$ law, the observed linear dependence for $H_{IC} = 400$ Oe has the highest slope and is shifted vertically toward longer switching times. Both characteristics show a noticeable degradation of the switching dynamics in case of moderate intergrain coupling.

As a function of the intergrain coupling (see Fig. 10) for a fixed writing pulse amplitude ($V = -0.35$ V), the relative switching duration clearly shows a transition from the weak to the strong coupling regime at $H_{IC} = 0.6$ kOe (approximately one-half of the ΔK_{1eff} distribution amplitude), with a flat dependence on both sides. On the strongly coupled side, the flat dependence means that the intergranular interaction strength is enough to maintain the collective macrospinlike dynamics. As a result, further increasing H_{IC} does not bring any additional effect. The flatness of the low$-H_{IC}$ side is just a consequence of the fact that for this given voltage, as seen in Fig. 9, there is no significant difference in the relative switching duration for $H_{IC} \leqslant 0.4$ kOe. The modification of the whole dependence with temperature is driven mainly by two factors: In the weakly coupled regime, the distribution of switching times of the individual grains increases faster than its mean value (t_0). In the strongly coupled regime, the situation is different: The whole ensemble reverses as a single macrospin, while the temperature spreads the switching duration. The thermal stability is higher in the strongly coupled regime. Lowering the temperature gives rise to a significant increase in switching time due to a reduction of the initial magnetic misalignment provided by thermal fluctuations. The initial spin torque is too

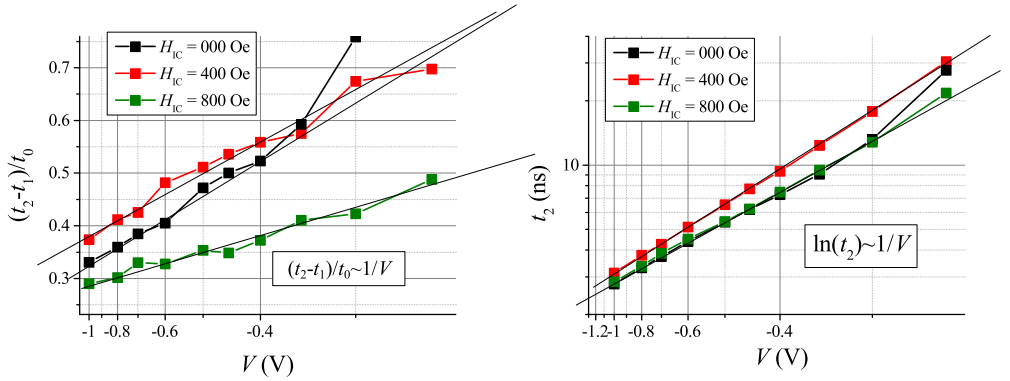

FIG. 9. Relative switching duration (left panel) and ensemble full switching time (right panel) for the different writing pulse amplitudes. Simulations are done for $T = 300$ K.

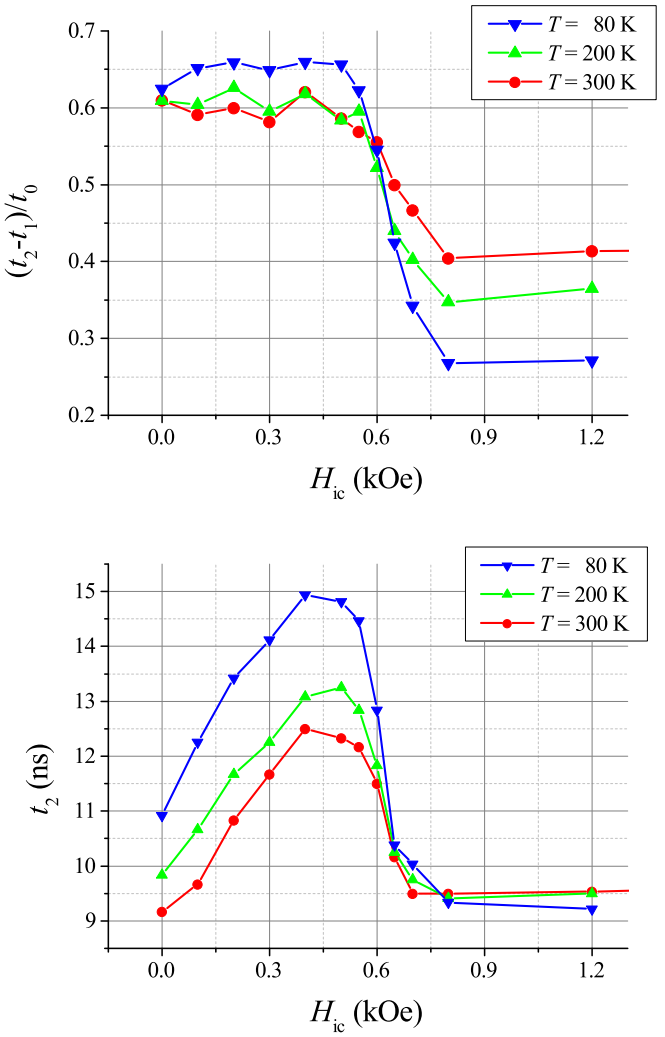

FIG. 10. Relative switching duration (top panel) and ensemble full switching time (bottom panel) for different interlayer coupling strengths. Simulations were carried out for $V = -0.35$ V.

small, and a great deal of time (so-called "incubation time") is needed to get a sufficiently large misalignment to trigger the magnetization reversal.

The full switching-time parameter shows a quite unexpected nonmonotonous variation versus H_{IC} (Fig. 10, bottom graph). The switching time increases with H_{IC} until it reaches a maximum in the weakly coupled regime, then it sharply drops at the transition to the strong coupling regime. Such dependence seems counterintuitive from the energetic point of view because the same volume of ferromagnetic material with the same total anisotropy energy should not dissipate more energy ($E \sim V^2 \cdot t_2$) for the switching, whether it is divided into subdomains or not (at least, considering that the thermal fluctuations are strong enough to remove the incubation time effect). To understand this issue, one has to analyze the spectral properties of the ensemble.

Once the grains are exchange-coupled, they acquire a collective dynamics represented by a set of eigenmodes. In case of ferromagnetic intergrain coupling, the lowest mode corresponds to the in-phase precession of all four macrospins. Its resonance frequency corresponds to the average of the

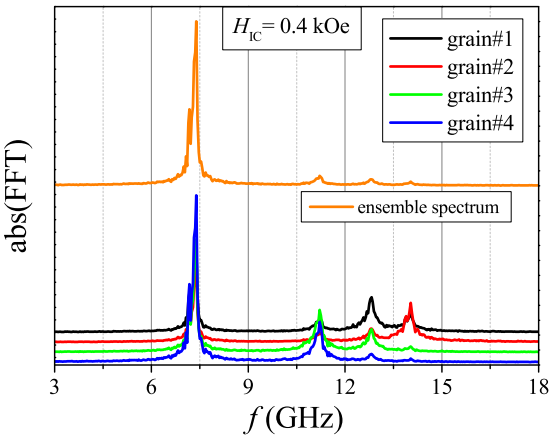

FIG. 11. FFT magnitude spectra of thermally excited FMR in each grain (black, red, green, and blue lines) and respective FFT spectrum of the whole ensemble (orange line).

weighted contribution of the four frequencies in the uncoupled case. Once the intergrain exchange field is large enough to overcome the grain-to-grain distribution of effective fields in the ensemble, further increasing the exchange does not change this excitation mode anymore. Other modes lying higher in the frequency spectrum correspond to modes in which the magnetic moments of the different grains precess out-of-phase with respect to each other. Their position in the frequency spectrum directly depends on the intergrain coupling strength, H_{IC}.

Figure 11 shows the thermally excited FMR spectra in the ensemble for $H_{IC} = 400$ Oe, $T = 80$ K. The thermal stochastic field, having a broad spectral range, excites simultaneously all possible FMR modes in the ensemble (the so-called thermally induced FMR). A relatively small STT amplitude ($V = -0.2$ V, significantly below the switching voltage) was also applied in order to increase the amplitude of the FMR signal. To obtain the FMR spectra, a LLG integration of the ensemble dynamics was performed for $t = 200$ ns. The time dependence of the transversal component of each macrospin was transformed by fast Fourier transform (FFT) into the frequency domain. The same procedure was repeated ten times to reduce the stochasticity (or just noise). Thus, each spectrum shown in Fig. 11 represents an average of ten FMR spectra. In addition to the individual FMR responses of each grain, the collective FMR response of the ensemble was obtained following the same procedure. Only the amplitudes of the FFT spectra are plotted in Fig. 11. The corresponding phase spectra will not be discussed; all the necessary conclusions will be derived by comparing individual and collective response spectra, where the phase difference influences the total amplitude.

Figure 11, calculated for $H_{IC} = 0.4$ kOe, shows that three exchange FMR modes are shifted away from the main acoustic mode (peak around 7 GHz), and their intensities are noticeably lower. The out-of-phase mutual precession between the grains is clearly seen by comparing the collective ensemble dynamics spectrum with the sum of the four individual spectra: obviously, the ensemble spectrum is not just an amplitude sum of the four individual amplitude spectra; the exchange mode

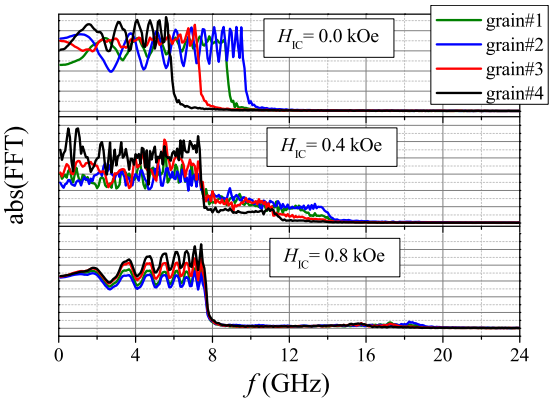

FIG. 12. FFT magnitude spectrum of the switching for each grain in the ensemble for zero, moderate, and strong intergrain coupling field. In order to avoid large phase noise, the temperature was reduced to $T = 20$ K.

peaks in the ensemble spectrum almost disappear due to their mutual out-of-phase oscillations. This situation is similar to a classical FMR in an exchange-coupled system, where the optical mode amplitude is dependent on magnetic asymmetry between two exchange-coupled subsystems.

The presence of these exchange modes during the STT switching process is responsible for the increase of the ensemble switching time in case of moderate intergrain coupling. Indeed, only the low-frequency acoustical mode absorbing the STT energy provides the increase in the precession angle of the net magnetic moment necessary for the switching. In contrast, the energy absorbed by the exchange modes only results in a partial decrease of the net magnetic moment magnitude. In other words, the increase of the switching time in the weakly coupled regime is linked to the fact that part of the STT energy is wasted to increase the system exchange energy due to excitation of the exchange modes.

The Fourier spectrum of the STT switching process at $T = 20$ K and $V = -0.5$ V clearly demonstrates this effect in Fig. 12. Three cases are represented:

(i) First, the case of the uncoupled ensemble is shown (top panel in Fig. 12). The STT reversal spectrum of each grain has a characteristic rectangular shape with a sharp high-frequency cutoff corresponding to the FMR frequency of each grain near the equilibrium—-it is the highest possible frequency, due to the inexistence of the exchange-coupled modes. The decrease of the precession frequency with increasing precession orbit during the STT switching fills more or less uniformly the low-frequency part of the spectrum. Different $K_{1\text{eff}}$ magnitudes in each grain result in different cutoff frequencies.

(ii) The second case corresponds to the moderate coupling regime (middle panel in Fig. 12). A broad range of excitations can be seen in the range between 10 and 14 GHz corresponding to the excitations of the exchange modes which were discussed above.

(iii) In the strongly coupled regime (bottom panel in Fig. 12), the STT reversal process is uniform; all the grains show the same spectral response reflecting their synchronous dynamics, while the exchange modes, being shifted to the higher frequencies (13–17 Ghz), have already negligible magnitudes and therefore do not participate in the STT switching dynamics.

An increase in the number of exchange modes in case of a larger number of grains should, in principle, lead to an even more pronounced effect, i.e., more energy will be dissipated in higher-order oscillations. The same behavior is expected in case of a continuous uniform free layer, if higher-order FMR excitations (drum modes, azimuthal modes, edge modes which are observed on single nanosized ferromagnetic disks [22,23]) have relatively high magnitudes with respect to the uniform mode. The thermal stability of the free layer is expected to degrade also due to a high probability of subvolume excitations, as was studied by Sun *et al.* [24].

At the level of a full-sheet free-layer film, the FMR signal in such granular ensemble should exhibit two main characteristic features which are actually observed in the experiments: a nonuniform broadening and a second-order magnetic anisotropy with a negative $K_{2\text{eff}}$ constant. One should notice that the simulated ensemble did not have a large grain-to-grain dispersion of the perpendicular-anisotropy field. Therefore, a quite small effective exchange field was needed to observe the exchange modes dynamics. Considering that both the second-order anisotropy and the degradation of the switching time are the largest for the system in which the exchange-field magnitude is comparable to the amplitude of the anisotropy field fluctuations, one can conclude that that the presence of the second-order magnetic anisotropy may be accompanied by a degradation of the STT switching characteristics due to exchange-mode excitations.

VI. CONCLUSIONS

We demonstrated a gradual onset of a granular behavior of the free layer when decreasing its nominal thickness. Below ~1.3 nm, the free layer behaves as an ensemble of weakly coupled ferromagnetic grains still having high perpendicular anisotropy but being already thermally unstable at $T = 300$ K due to a noticeable decrease of the activation volume. In thicker layers, the increase of the intergrain exchange rapidly favors a "macrospinlike" behavior of the free layer. Nevertheless, even in these thick films, the temperature-dependent FMR measurements reveal quite strong fluctuations of the free-layer magnetic parameters. The increase of the intergrain exchange with the nominal free-layer thickness causes the emergence of a second-order anisotropy term, in line with its micromagnetic nature (spatial fluctuations of the first-order uniaxial anisotropy) [10].

Taking into account the grain-to-grain distribution of the perpendicular anisotropy, a moderate intergrain coupling yields the maximum amplitude of second-order anisotropy term. At the same time, the moderate coupling worsens the STT switching characteristics of the free layer. Therefore, relying on the spatial fluctuations of the uniaxial anisotropy as a source of the second-order anisotropy seems not to be the best way to induce the easy-cone magnetic state in the free layer.

We can summarize our findings as follows:

(1) The magnetic and magnetotransport properties of pMTJ and their variation with the free-layer thickness can be described by a granular film model with three main parameters

influenced by the nominal layer thickness: mean grain magnetic anisotropy, grain-to-grain anisotropy distribution, and intergrain exchange-coupling strength.

(2) A thickness-dependent study of magnetoresistive and magnetoresonance properties of the free layer revealed a direct correlation between the degree of the film granularity (characterized by the intergrain coupling), the higher-order magnetic anisotropy constant, and the inhomogeneous broadening of the FMR line. Magnetic inhomogeneities with spatial period larger than the exchange length contribute to the inhomogeneous FMR line broadening; those which are comparable to the exchange length additionally yield the second-order magnetic anisotropy with a negative constant.

(3) Moderate exchange coupling increases the magnitude of the higher-order anisotropy term but simultaneously degrades the switching characteristics of the free layer because of the excitation of exchange modes which reduce the STT switching efficiency of the free layer.

Therefore, to improve the STT MRAM switching performance, it may be preferable not to rely on the second-order anisotropy due to spatial fluctuations of the first-order anisotropy but rather on that existing in bulk form, possibly in some Heusler alloys such as Mn_2RhSn [25], or on using suitably chosen exchange-coupled layers such as in exchange-coupled media used in magnetic recording.

ACKNOWLEDGMENTS

The work was partially supported by the Samsung Global MRAM Innovation Program, CEA-EUROTALENTS fellowship (A.A.T.), ERC Advanced Grant MAGICAL No. 669204, French National Research Agency (ANR) under Project No. EXCALYB. N.A.S. and B.M.S.T. acknowledge financial support of the FCT of Portugal through the Project No. I3N/ FSCOSD (Ref. FCT UID/CTM/50025/2013) and through the bursary PD/BD/113944/2015. The samples used in this study were patterned in the PTA clean-room in Grenoble (Upstream research nanofabrication platform).

[1] P. A. Algarabel, A. D. Moral, M. R. Ibarra, and J. I. Arnaudas, J. Phys. Chem. Solids **49**, 213 (1988).
[2] B. M. S. Teixeira, A. A. Timopheev, R. Schmidt, M. R. Soares, M. Seifert, V. Neu, and N. A. Sobolev, J. Phys. D: Appl. Phys. **49**, 315002 (2016).
[3] R. Matsumoto, H. Arai, S. Yuasa, and H. Imamura, Phys. Rev. B **92**, 140409 (2015).
[4] N. Strelkov, A. Timopheev, R. C. Sousa, M. Chshiev, L. D. Buda-Prejbeanu, and B. Dieny, Phys. Rev. B **95**, 184409 (2017).
[5] R. Matsumoto, H. Arai, S. Yuasa, and H. Imamura, Phys. Rev. Appl. **7**, 044005 (2017).
[6] H. Arai, R. Matsumoto, S. Yuasa, and H. Imamura, Appl. Phys. Express **8**, 083005 (2015).
[7] A. A. Timopheev, R. Sousa, M. Chshiev, H. T. Nguyen, and B. Dieny, Sci. Rep. **6**, 26877 (2016).
[8] J. M. Shaw, H. T. Nembach, M. Weiler, T. J. Silva, M. Schoen, J. Z. Sun, and D. C. Worledge, IEEE Magn. Lett. **6**, 3500404 (2015).
[9] Y. Fu, I. Barsukov, J. Li, A. M. Gonçalves, C. C. Kuo, M. Farle, and I. N. Krivorotov, Appl. Phys. Lett. **108**, 142403 (2016).
[10] B. Dieny and A. Vedyayev, EPL **25**, 723 (1994).
[11] L. Cuchet, R. C. Sousa, L. Vila, S. Auffret, B. Rodmacq, and B. Dieny, IEEE Trans. Magn. **50**, 1 (2014).
[12] J. M. Teixeira, J. Ventura, J. P. Araujo, J. B. Sousa, P. Wisniowski, and P. P. Freitas, Appl. Phys. Lett. **96**, 262506 (2010).
[13] V. Drewello, J. Schmalhorst, A. Thomas, and G. Reiss, Phys. Rev. B **77**, 014440 (2008).
[14] R. Berger, J.-C. Bissey, J. Kliava, H. Daubric, and C. Estournès, J. Magn. Magn. Mater. **234**, 535 (2001).
[15] J. Z. Sun, Phys. Rev. B **91**, 174429 (2015).
[16] E. Callen and H. Callen, Phys. Rev. **129**, 578 (1963).
[17] H. Callen and E. Callen, J. Phys. Chem. Solids **27**, 1271 (1966).
[18] W. Kipferl, M. Sperl, T. Hagler, R. Meier, and G. Bayreuther, J. Appl. Phys. **97**, 10B313 (2005).
[19] M. Sperl, W. Kipferl, M. Dumm, and G. Bayreuther, J. Appl. Phys. **99**, 08J703 (2006).
[20] D. Apalkov and D. Druist, Inventors; Samsung Electronics Co., Ltd., assignee. US Patent No. 8,704,547 (22 April 2004).
[21] W. F. Brown, Jr., Phys. Rev. **130**, 1677 (1963).
[22] V. V. Naletov, G. de Loubens, G. Albuquerque, S. Borlenghi, V. Cros, G. Faini, J. Grollier, H. Hurdequint, N. Locatelli, B. Pigeau, A. N. Slavin, V. S. Tiberkevich, C. Ulysse, T. Valet, and O. Klein, Phys. Rev. B **84**, 224423 (2011).
[23] T. Devolder, J.-V. Kim, L. Nistor, R. Sousa, B. Rodmacq, and B. Diény, J. Appl. Phys. **120**, 183902 (2016).
[24] J. Z. Sun, R. P. Robertazzi, J. Nowak, P. L. Trouilloud, G. Hu, D. W. Abraham, M. C. Gaidis, S. L. Brown, E. J. O'Sullivan, W. J. Gallagher, and D. C. Worledge, Phys. Rev. B **84**, 064413 (2011).
[25] O. Meshcheriakova, S. Chadov, A. K. Nayak, U. K. Rößler, J. Kübler, G. André, A. A. Tsirlin, J. Kiss, S. Hausdorf, A. Kalache, W. Schnelle, M. Nicklas, and C. Felser, Phys. Rev. Lett. **113**, 087203 (2014).